04,13

Complex experimental and theoretical study of KIn_5S_8 crystals: vibrational and thermodynamic properties

© E.A. Pankrushina[1], E.M. Roginskii[2,¶], D.A. Chareev[3], G.S. Ilin[4], S.L. Votyakov[1]

[1] Zavaritsky Institute of Geology and Geochemistry, Ural Branch of the Russian Academy of Sciences, Yekaterinburg, Russia
[2] Ioffe Institute, St. Petersburg, Russia
[3] Korzhinskii Institute of Experimental Mineralogy, Russian Academy of Sciences, Chernogolovka, Russia
[4] Federal Research Centre Kola Science Centre of the Russian Academy of Sciences (FRC KSC RAS), Apatity, Russia

¶ E-mail: e.roginskii@mail.ioffe.ru, lizaveta.94@list.ru

Received December 23, 2025
Revised January 6, 2026
Accepted January 14, 2026

The structural and dynamic properties of the KIn_5S_8 crystal were studied experimentally and theoretically using the density functional theory. Single-crystal X-ray diffraction analysis allowed us to refine the structural parameters of the crystalline phase with the space group *C2/m* (N 12), while quantum chemical calculations predict the coexistence of three low-temperature phases, namely *P-1* (N 2), $P2_1$ (N 4), $P2_1/c$ (N 14). Using the quasi-harmonic approximation for KIn_5S_8 at 300 K, the values of the thermal expansion coefficient ($3.90 \cdot 10^{-5}\,K^{-1}$) and the bulk modulus (37.23 GPa) were obtained. The Debye temperature θ_D was also determined, which allowed us to estimate, using the empirical Slack-Morelli formula, the lattice thermal conductivity due to phonon-phonon interaction, which was $\kappa_L = 0.41$ W/(mK) at 300 K. For the first time, the temperature and pressure dependences of the Raman spectra of KIn_5S_8 were experimentally obtained in situ and analyzed. A strong manifestation of anharmonicity of vibrational modes in the center of the Brillouin zone was revealed, indicating the potential of using KIn_5S_8 crystals in the field of phonon engineering of anharmonicity.

Keywords: Raman spectroscopy, DFT, chalcogenides, anharmonicity, thermal conductivity.

DOI: 10.61011/PSS.2026.01.63241.8925-25

1. Introduction

The interaction of different types of vibrations (phonons) in a crystal has a decisive effect on the physical properties, the reaction of the material to external energy influences (temperature, pressure) and, ultimately, on its behavior as a functional material in certain technological processes. The origin of deformations caused by temperature and pressure is different, but in both cases it is associated with potential anharmonicity. In recent years, the concept of anharmonicity engineering [1] — regulation of heat transfer to achieve the necessary characteristics of materials has been introduced in the literature. By increasing the number of defects, external compression or lattice stress, it is possible to control the lattice anharmony, while controlling the properties of the material. In practice, this manifests itself as a number of new phenomena caused by phonon anharmonic effects, such as ferroelectric phase transition, negative thermal expansion, ultra-low thermal conductivity, etc., which makes the concept of anharmonic engineering increasingly relevant both in fundamental research and in practical applications. However, this direction is at the stage of formation; many questions remain open, in particular, the issues of quantifying the Grüneisen mode parameters as a measure of anharmonicity, the state of chemical bonding in crystals, etc. In recent years, anharmonicity has been studied using a number of modern methods, including theoretical, experimental, and computational methods, which have provided new insights into the microscopic mechanisms of anharmonicity [2–4]. Raman spectroscopy provides similar information about phonon anharmonicity as inelastic neutron scattering in the center of the Brillouin zone, but with a number of advantages, such as high resolution and the ability to study micron samples [3,5–7]. Theoretical modeling *ab initio*, based on the widely used density functional theory (DFT), is indeed a powerful tool for this kind of research, allowing simultaneous description of high temperatures and pressures [8,9]. *Ab initio* prediction of the thermal conductivity of the lattice (κ_L) of crystals is an urgent task for solid state physics. Chalcogenides, and in particular sulfides, are characterized by complex donor-acceptor bonds that are intermediate between ionic, covalent, and metallic, and they manifest themselves in different ways in the lattice volume. Cations and anions tend to form stable outer electron shells of inert gases in the structure of sulfides, which is often realized by socializing electrons. Such properties make them interesting in terms of potential photovoltaic materials and applications in photo-

voltaics. Current trends are focused on the so-called alkaline pnictogenic dichalcogenides I-V−VI2 (alkali metal — pnictogen [Bi, Sb, As] — chalcogen [S, Se, Te]) [10], which are considered promising semiconductor materials for energy conversion devices, the defining properties of which are lone electron pairs (typical for Bi^{3+}, Sb^{3+}, As^{3+}). Interesting data were obtained in Ref. [11] for a compound of a similar type — $CuInTe_2$, where, combining Raman Spectroscopy and DFT, the authors explained the anomalous drop in its lattice thermal conductivity κ_L at high temperatures (which is typical for this type structures) and proposed methods for controlling κ_L by changing phonon modes using external compression or lattice voltage. An unusual system is the chalcogen metals of the 13th group in combination with alkali metals. These compounds have long been of great interest in solid state chemistry, which has led to numerous scientific papers such as Refs. [12–15]. For example, the compounds $LiMX_2$ (M = Ga, ln; X = S, Se) [16–19], BaM_4X_7 (M = Al, Ga; X = S, Se) [20–23]) have a very large nonlinear optical response in the IR range; compounds $BaGa_2X_4$ (X = S, Se) [24,25] have been widely studied as luminescent materials. Family of AB_5X_8 [26] (A = Cu or Ag, B = In and X = S, Se or Te) is one of the most important representatives among ternary semiconductors, due to the fact that some of them are characterized by ultra-low values of κ_L, such as for $AgIn_5S_8$ and $CuIn_5S_8$, the values of κ_L correspond to 0.29 and 0.54 W/(mK) at 1000 K. However, there is practically no information in the literature about the properties of such compounds as MIn_5X_8 (M = alkali metal, X = S, Se). They were indirectly discussed in Daniel Friedrich's dissertation [27], while other papers are mainly devoted to their synthesis and date back to the last century [28,29]. To date, it is known that saturated yellow and transparent single crystals of ternary thioindates MIn_5X_8 (M = K, Rb, Cs) crystallize in the monoclinic space group $C2/m$ ($Z = 2$). They are characterized by a three-dimensional network of InS_6 octahedra forming parallel channels completely filled with alkali metal ions. A characteristic feature of the structure is the alternation of two layers consisting exclusively of S^{2-} ions, with a layer consisting of M^+ and S^{2-} (MS_2). Only the octahedral cavities between the layers, consisting exclusively of S^{2-} (S3) ions, are completely filled with In^{3+} ions. The octahedral cavities between the mixed (MS_2) and pure layers S^{2-} are partially filled with ions In^{3+}, which avoids direct contact with ions K^+. The octahedral coordination around In^{3+} exhibits pronounced (4+2)-coordination, described as distorted tetrahedral. The central perspective projections of sulfur coordination polyhedra around alkali metal cations indicate a decrease in the anisotropy of thermal fluctuations during the transition from a potassium compound to a cesium compound [28]. Ion K^+ does not fill the existing cavity in the structure well, unlike ions Rb^+ and Cs^+, and deviates into acentric separated positions. This may also be the reason that the compound $NaIn_5S_8$ has not yet been obtained, because the ion Na^+ is too small [28]. According to the MaterialsProject [30] database, the band gap for $CsIn_5S_8$, $RbIn_5S_8$, KIn_5S_8 is ~ 1.2 eV. Thus, the purpose of this work is to study the manifestations of its dynamic and thermodynamic properties in Raman spectroscopy beyond the harmonic model using the example of the synthetic crystal KIn_5S_8 as part of the development of the scientific field of anharmonicity engineering. To understand phonon anharmonicity, it is necessary to analyze the local structure of the material, its temperature and baric evolution, and determine the stability ranges and electronic structure. Such data are necessary in analyzing the properties of thermoelectrics, ferroelectrics, multiferroics, high-temperature superconductors, etc. Due to the importance of the phenomenon of phonon anharmonicity for modern materials, it is necessary to comprehensively study them.

2. Experimental procedure

KIn_5S_8 crystals were obtained in eutectic melts of alkali metal salts in a stationary temperature gradient [31,32]. Powdered In_2S_3 was prepared in evacuated quartz glass ampoules at 920 K. Metallic In and crystalline S were used as precursors. Anhydrous Na_2S was obtained from hydrated $Na_2S \cdot xH_2O$, heated under vacuum on a smoking burner flame. The reaction vessel for obtaining crystals was an ampoule of quartz glass, which was located in a furnace in a temperature gradient. The temperature of the hot end was 1040 K, the cold end — about 70 K lower. In the hot part of the reaction vessel there was a charge $In_2S_3 + Na_2S$ taken in a molar ratio of 4 : 1, which gradually dissolved in the salt melt KCl/KBr/KI, migrated to the cold the end of the ampoule formed crystals there with the participation of potassium atoms, not sodium. The formation of phases with the participation of the heaviest alkali metal is almost a general rule during crystallization in various salt mixtures with the participation of alkali metals [32]. The crystals continued to grow for about four weeks. After the synthesis was completed, the ampoules were removed from the furnace and cooled in water. Parts of ampoules with crystals were dissolved in distilled water, alcohol, and acetone using an ultrasonic washer. Then the product was dried in a muffle at a temperature of 340 K for several minutes. As a result, orange needle-like crystals up to 5 mm long were obtained.

Single crystal X-ray diffraction data was performed at room temperature using a Rigaku XtaLABSynergy-S diffractometer (MoKα — radiation, graphite monochromator, Hybrid Pixel Array detector). Refinement of the unit cell parameters, data integration, and correction for background radiation, the Lorentz factor, and polarization were performed using the CrysAlis software package version 1.171 (Oxford Diffraction Crysalis Pro. Oxford Diffusion Ltd, Abingdon, Oxfordshire, UK, 2009). The refinement of the structure was performed using the JANA2006 software [33].

Raman spectra in a wide frequency range ($0-500\,cm^{-1}$) were measured in backscattering geometry using a Horiba LabRam HR800 Evolution spectrometer (1800 diffraction

grating,gr/mm) equipped with an OlympusBX-FM and a charge-coupled detector cooled by the Peltier effect to ~ 200 K. A He-Ne laser (radiation wavelength 633 nm, laser power 1 mW) was used as the excitation source. No photoluminescence was observed in all experimental Raman spectra. The spectra were recorded using an Olympus lens $50\times$ (numerical aperture (NA) $= 0.7$) by collecting data for 50 s with two accumulations for each segment of the spectrum. The spectrometer was calibrated by setting the position of the Rayleigh line and using a neon lamp (Horiba). The polarized spectra of KIn_5S_8were measured on a Horiba T64000 spectrometer in three experimental geometries $Z(XX)\bar{Z}$, $Z(YY)\bar{Z}$, $Z(XY)\bar{Z}$, which cover the entire set of phonons allowed in Raman spectra. The study of Raman spectra *in situ* in the temperature range of 83–773 K was carried out using a Linkam TSM 600 thermal cell (heating rate was 20 K/h, temperature step 10–20 K). Raman Spectroscopy *in situ* experiment at pressures up to ~ 10 GPa was performed using a cell with an Evolution Diacell diamond anvilμScopeDAC-HT[G] and a gas membrane. An inconel gasket with a thickness of 250 μm, compressed to a thickness of 80 μm, with a hole with a diameter of 150 μm was used. The pressure in the cell was determined using ruby photoluminescence lines (lines $R1$ and $R2$). In the experiments, a mixture of methanol-ethanol alcohols was chosen as the pressure-transmitting medium (1 : 4) [34].

3. Computing technique

The calculations of the phonon spectra were carried out within the framework of the density functional theory implemented in the VASP [35,36] software package, using a generalized gradient approximation with the PBE functional [37] and the pseudopotential method. The 3p4s3d electronic states were considered as valence states for K atoms, and the 5s5p5d4 and 3s3p3d states were considered as valence states for In and S atoms, respectively. The interactions between the nucleus and valence electrons were described using the projector augmented wave (PAW) method [38.39]. The completeness of the basic set was controlled using the cutoff energy E_{cut}, equivalent to 550 eV. The Brillouin zone was integrated in the reverse space on a grid $2\times2\times1$ selected according to the Monkhorse-Pack scheme [40]. The Raman spectra were modeled using calculations of the Raman tensor for each vibrational mode within the framework of the coupled perturbed Hartree-Fock model (CPKS) [41] implemented in the CRYSTAL14 software package [42] using full-electron basis sets with triple zeta valence [43] and the PBEsol functionality [44]. A complete optimization of the geometric parameters of the cell and the position of the atoms was performed as an initial step before calculating the electronic and vibrational properties. The lattice parameters were relaxed until the pressure value became less than 0.01 GPa, and the position of the atoms was optimized until the forces acting on the atoms remained at the level of 10^{-3} eV/Å. The dispersions of the phonon branches were calculated using an extended cell. The following transition matrix from elementary to extended cell $\begin{pmatrix}1 & -4 & -1\\ 1 & 4 & -1\\ 1 & 0 & 1\end{pmatrix}$ was used, and the vibrational properties were studied by solving the problem of searching for eigenvectors and values of a dynamic matrix constructed from force constants calculated by the finite difference method as implemented in the PHONOPY package [45]. The thermodynamic characteristics were calculated using the quasi-harmonic approximation (QHA) [46].

Table 1. Experimental and calculated lattice parameters KIn_5S_8 with symmetry $C2/m$

Parameter	Experiment	Calculation
a, Å	19.048(1)	19.153
b, Å	3.845(8)	3.839
c, Å	9.211(5)	9.1890
β	103.312(1)	103.284
V, Å^3	656.658(9)	657.657

4. Experimental results

4.1. Single crystal X-ray diffraction

In order to determine the structural parameters, single crystal X-ray diffraction analysis of KIn_5S_8 was performed. The structure was refined in the spatial group *C2/m* to the final value $R = 2.19\,\%$ in the anisotropic approximation of atomic displacements using 819 reflections with $I > 3\sigma(I)$ using the JANA2006 program. The structure of KIn_5S_8 is shown in Figure 1. It is worth noting that the crystal structure is composed of InS layers, between which there are binding alkali metal atoms K. Each layer is made up of endless chains of In and S atoms stretched along the crystallographic axis b as shown in Figure 1. Two types of chains can be distinguished, the so-called „mono-ladders“, highlighted in purple, in which the bonds of atoms In-S form steps, and „bi-ladder“, shown in blue in Figure 1.

The optimization of the structural parameters KIn_5S_8 was performed in this paper within the framework of density functional theory (DFT). The obtained values of the monoclinic cell parameters, in comparison with the experimental data, are plotted in Table 1. In general, there is a good agreement between experiment and theory, which indicates the correctness of the chosen calculation scheme.

4.2. Structural and dynamic properties

Dynamic properties were calculated and analyzed to assess the nature of the vibrational modes KIn_5S_8.

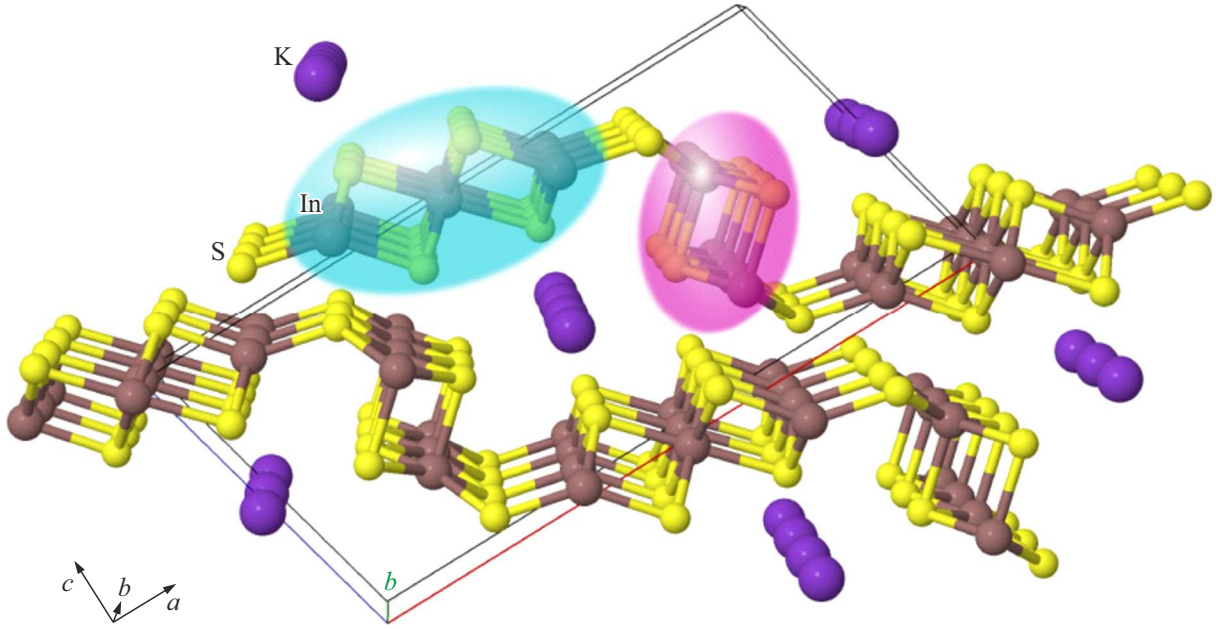

Figure 1. Spatial structure of KIn_5S_8. Purple circles — potassium atoms, yellow and brown circles — sulfur and indium atoms, respectively.

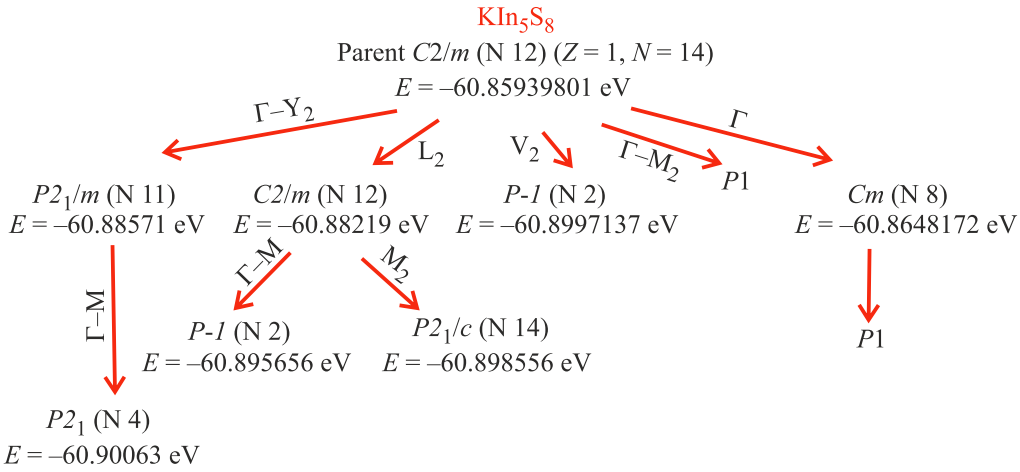

Figure 2. Diagram „group-subgroup“ for KIn_5S_8 and the total energy of structures E, eV.

If we assume that KIn_5S_8 crystallizes in the space group $C2/m$, then we should consider the vibrational representation in the center of the Brillouin zone as $\Gamma_{optic} = 12A_g + 7A_u + 6B_g + 14B_u$. The dispersion of the phonon branches was calculated along a highly symmetric path V_2-Γ-C_2–Y_2-Γ–M_2- D-A-Γ-L_2 in the Brillouin zone. However, in DFT calculations of the dispersion of the phonon branches of the crystal KIn_5S_8, a completely imaginary branch was found. It is worth noting that this is an optical branch with Bu symmetry. Taking into account the contradictions in the data on the crystal structure of KIn_5S_8, an attempt was made to find a stable structure of this material with a spatial symmetry different from $C2/m$ (N 12). Using the standard approach [47], and previously tested on similar systems [48], which assumes the displacement of atoms along the normal coordinates of an unstable mode with an imaginary frequency, and following the diagram „group–subgroup“ shown in Figure 2, a set of phonon spectra and phonon densities of states was obtained. The calculated total energies and the absence of imaginary phonon frequencies in the phonon spectrum for KIn_5S_8 indicate several stable structures from the point of view of DFT calculation, namely *P-1* (N 2), $P2_1$ (N 4), $P2_1/c$ (N 14) (Figure 2).

Based on all of the above and according to the results presented in Table 1, the decomposition of the vibrational spectrum into irreducible representations (IR) is as follows: $\Gamma_{optic} = 83A + 82B$ for KIn_5S_8 (given for the structure

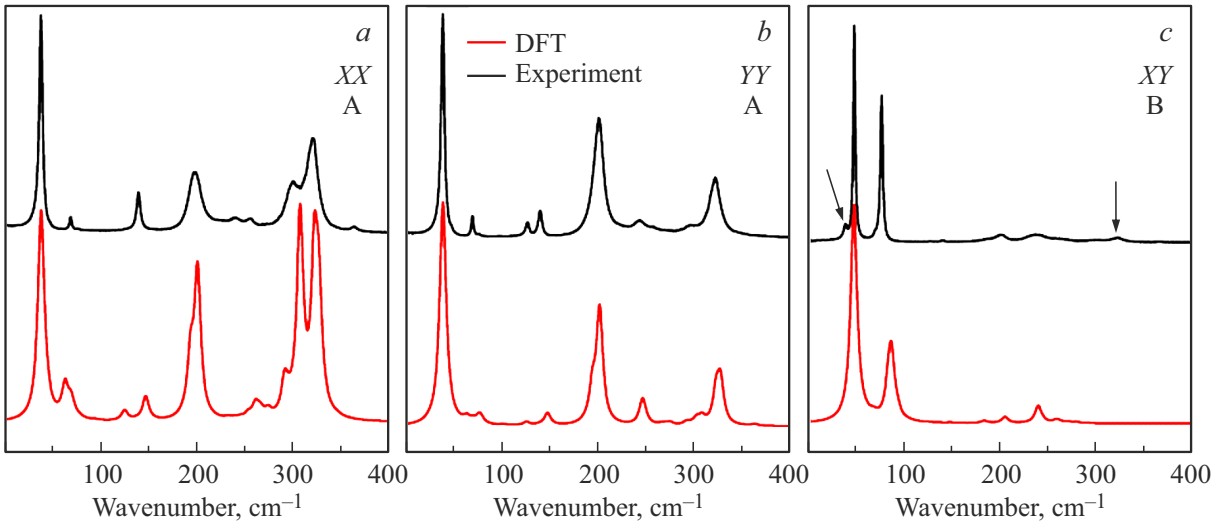

Figure 3. Calculated (DFT) and experimental (Exp.) Raman spectra of KIn_5S_8 in polarizations $Z(XX)\bar{Z}$ (*a*), $Z(YY)\bar{Z}$ (*b*), $Z(XY)\bar{Z}$ (*c*). The arrow points to a line that appears due to the effect of partial depolarization.

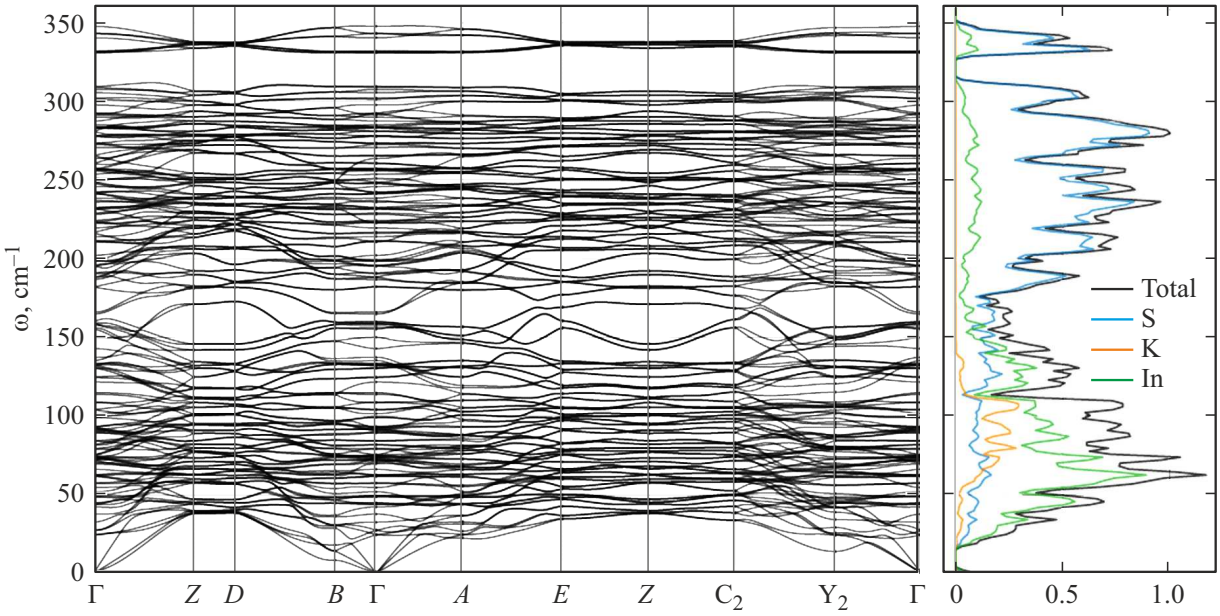

Figure 4. Dispersions of phonon branches and densities of phonon states of the crystal of KIn_5S_8 (spatial group $P2_1$).

$P2_1$, as the most stable in energy). Figure 3 shows the calculated Raman spectra. For KIn_5S_8, a superposition phonon spectrum is presented, reflecting the coexistence of several phases: *P-1* (N 2), $P2_1$ (N 4) and $P2_1/c$ (N 14). Calculations of dynamic properties at the Γ-point of the Brillouin zone are presented in Table 2 in comparison with experimentally obtained values. To better understand the role of each atom in each phonon mode, the phonon densities of states (PDOS) were calculated over the entire Brillouin zone (Figure 4). It is clearly seen that the greatest contribution to the low-frequency phonon modes (up to 100 cm^{-1}) is due to the displacements of In atoms, accompanied by small displacements of K. In the range from about 100 to 170 cm^{-1}, the contribution of the alkali metal is absent or at a minimum level, while the contributions of In and S predominate. The high-frequency range is characterized by a significant contribution of S to the vibration. At the same time, there is only a small participation of In. An analysis based on a comparison of the partial density of states with the total single-phonon density of states shows that several pronounced peaks in the single-phonon density of states can be uniquely associated with the specific dynamic behavior of structural units. It should be noted that in the KIn_5S_8 structure, the layers are formed from infinite chains In-S, which are located in the plane *ac* and are interconnected by a bridge atom S, which is considered

Table 2. Comparison of calculated phonon frequencies (cm^{-1}) at the Γ-point of the Brillouin zone of the KIn_5S_8 crystal with experimental Raman scattering data (exp.)

KIn_5S_8 (Exp.)		KIn_5S_8 (Calculation.)	
A	*B*	*A*	*B*
38.9	48.3	39.3	47.8
69.8	70.7	63.9	66.7
77.8	76.6	70	86.8
126.8	187.6	76.6	182.9
140.1	200.5	147.6	204.6
195.4	236.8	194.1	238.8
201	261.5	201.3	259
221	–	220	269.8
240.3	–	247.5	277.8
255.9	–	262.8	–
286	–	274.4	–
299.8	–	292.2	–
315.8	–	307.6	–
321.7	–	322.4	–
–	–	327	–
363.7	–	367	–

as „ladder steps“. In Figure 1 „ladder steps“ directed along the axis *b* are highlighted in red; „two-step“ are highlighted in blue. In this regard, analyzing the data from DFT calculations, all vibrations can be conditionally divided into several groups: atomic displacements in the „mono-ladder“, in the „bi-ladder“, and simultaneously in both (in these cases, the bridging S-bond may also either participate or not participate). In some cases, vibrations of In-S chains are accompanied by displacements of K atoms.

4.3. Raman spectroscopy

The polarized spectra of KIn_5S_8 were recorded in three experimental geometries $Z(XX)\bar{Z}$, $Z(YY)\bar{Z}$, $Z(XY)\bar{Z}$, (Figure 3). This set allows identifying vibrational modes in the spectra (IR *A* and *B*) allowed by the selection rules for KIn_5S_8. There is a good agreement between the calculations and the experiment, due to the well-reproducible interatomic distances (Table 2).

Vibrational modes transformed by IR *A* are active in the spectra with polarization $Z(XX)\bar{Z}$ and $Z(YY)\bar{Z}$. The low-frequency range up to $\sim 100\,cm^{-1}$ for the crystal of KIn_5S_8 is characterized by the presence of two peaks ~ 38 and $69\,cm^{-1}$. According to the DFT data, these vibrations are related to the pendulum vibrations of the atoms „mono-ladder“ and „bi-ladder“, including the displacements of the atom K ($\sim 38\,cm^{-1}$) and the predominant displacements of the In atoms in „mono-ladder“ and „bi-ladder“, accompanying the displacements of the atom of K ($\sim 69\,cm^{-1}$). The spectral peak at $\sim 38\,cm^{-1}$ is the most intense in the spectrum, while the peak at $\sim 69\,cm^{-1}$, on the contrary, is one of the weakest. Further, two weak peaks ~ 77 and $126\,cm^{-1}$ can be observed in the experimental spectrum, which, according to DFT, characterize vibrations of In atoms in the „mono-ladder“ cluster with the participation of K vibrations. Further, in the spectral range of $130-140\,cm^{-1}$, there is one peak at $\sim 140\,cm^{-1}$; it is associated with scissor vibrations of the „mono-ladder“ and bridge sulfur. In addition, the spectral range of $180-200\,cm^{-1}$ contains two poorly resolved peaks at ~ 195 and $201\,cm^{-1}$ associated with collective movements of „bi-ladders“, „mono-ladders“ and bridging sulfur; these modes can basically be described as pendulum vibrations. The range $220-260\,cm^{-1}$ contains a group of low-intensity peaks: $\sim 221\,cm^{-1}$ characterizes the collective torsional vibration of „bi-ladders“ and „mono-ladders“; at ~ 240, $255\,cm^{-1}$ correspond to the rocking vibrations in the „mono-ladder“ and „bi-ladder“. The mode with frequency of $\sim 286\,cm^{-1}$ is characterized according to DFT data as a stretching collective vibration of atoms „mono-ladder“ and „bi-ladder“. In the range of $290-330\,cm^{-1}$ there is a group of intense wide peaks ~ 299, 315, $321\,cm^{-1}$, characterizing the bending vibrations of atoms of „mono-ladder“ and „bi-ladder“. Finally, in the range above $350\,cm^{-1}$, there is one peak in the spectrum $\sim 363\,cm^{-1}$, corresponding to the vibration of the bridge S.

IR-transformed modes *B* manifest themselves in spectra with $Z(XY)\bar{Z}$ polarization. In this case, it is more convenient to consider vibrations in separate atomic layers, where the „mono-ladder“ layer contains alkali metal atoms (layer 1), and the „bi-ladder“ layer does not contain alkali metal atoms (layer 2). The low frequency range up to $\sim 100\,cm^{-1}$ is characterized by the presence of several high-intensity peaks: ~ 48, 70, $76\,cm^{-1}$, where the lowest frequency vibration is associated with the movements of the layer 2, while the vibration with the frequency $\sim 70\,cm^{-1}$ is associated with the active movement of the In atom in layer 1, the vibration at $\sim 76\,cm^{-1}$ is associated with an offset of K. In addition, the spectral range of $170-270\,cm^{-1}$ contains four low-intensity peaks: ~ 187, 200, 236, $261\,cm^{-1}$, where the atoms exhibit vibrations in the following order of layers: 1st layer, 2nd layer, 1st layer and scissor vibrations of „mono-ladder“ and „bi-ladder“The remaining peaks observed in the experimental spectra are associated with partial depolarization.

4.4. Temperature and baric dependence of the Raman spectra of KIn_5S_8

A series of measurements of the Raman spectra of single crystals KIn_5S_8 were conducted in this study, including

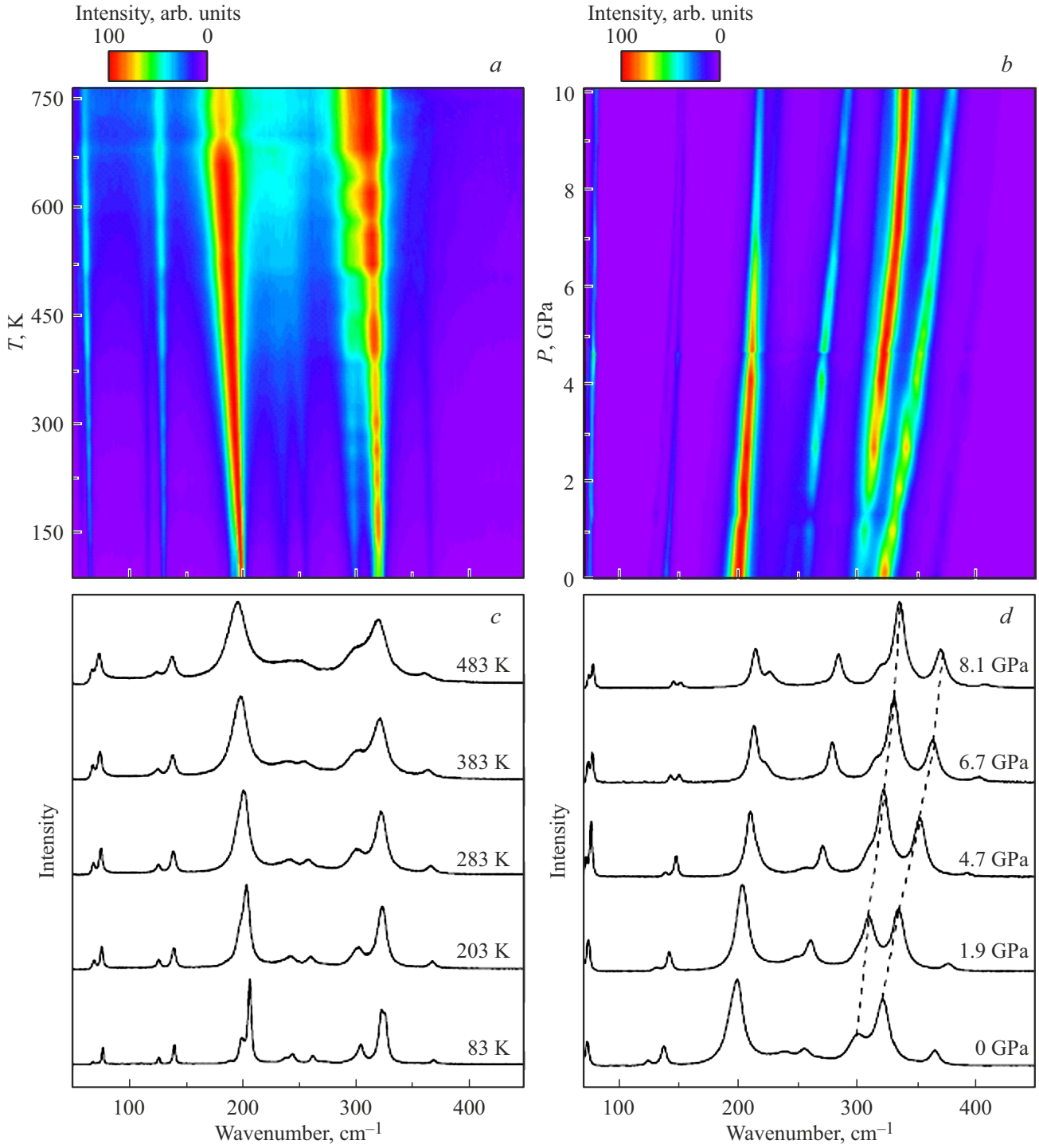

Figure 5. Temperature (a) and baric (b) dependences of the Raman spectra of the crystal of KIn_5S_8 in the temperature range of 83–773 K and pressure up to $\sim$ 10 GPa. Spectra of KIn_5S_8 at temperature of 83, 203, 283, 383, 483 K (c) and pressure of 0, 1.9, 4.7, 6.7, 8.1 GPa (d).

measurements in the temperature range of 83–773 K. In the Raman spectra, with increasing temperature, there is a broadening of most vibrational modes and a shift to the low-frequency region, as well as a change in the intensity of the lines (Figure 5). This sample is stable in the studied temperature range. However, it was possible to identify some features. In the spectral range of 100–370 cm^{-1}, most peaks are characterized by a rather large shift, on average $\omega \sim 15\,cm^{-1}$, and broadening, on average $\Delta\omega \sim 20\,cm^{-1}$. The highest frequency spectral peak of $\sim 363\,cm^{-1}$, characterizing the vibrations of the bridge S, is characterized by a maximum temperature shift (up to

$\sim 17\,cm^{-1}$). This is probably due to less strong bonds in the interlayer space than in the layers. The spectral peak $\sim 255\,cm^{-1}$ is characterized by a rather large broadening $\Delta\omega \sim 18\,cm^{-1}$. The most stable in temperature are the low-frequency vibrations $\sim 140\,cm^{-1}$, for which minimal shift and minimal broadening are observed.

The temperature-dependent frequency of the mode has a volumetric and true/explicit anharmonic contribution, which can also be expressed as follows:

$$\omega(T) = \omega_0 + \Delta\omega_{vol}(T) + \Delta\omega_{anh}(T), \quad (1)$$

where $\omega(T)$ is the frequency of the Raman mode at temperature T, ω_0 is the frequency at absolute temperature, $\Delta\omega_{vol}(T)$ is the volumetric/quasi-harmonic contribution (or the implicit contribution discussed previously) in the frequency shift, and $\Delta\omega_{anh}(T)$ is a true/explicit anharmonic contribution to the frequency shift. It is caused by the third, fourth and higher degrees of decomposition of the interatomic potential according to the degrees of displacement of atoms from equilibrium positions [49,50].

$$\Delta\omega_{anh}(T) = \omega_0 + A\left(1 + \frac{2}{(e^x - 1)}\right) + B\left(1 + \frac{3}{(e^y - 1)} + \frac{3}{(e^y - 1)^2}\right), \quad (2)$$

where $x = \hbar\omega_0/2kT$; $y = \hbar\omega_0/3kT$.

Spectral lines exhibit broadening at high temperatures due to three and/or four-phonon processes. The full width at half maximum in the Raman spectrum (FWHM) due to three- and four-phonon decay processes at higher temperatures are determined by the expression [49]

$$\Gamma(T) = \Gamma_0 + C\left(1 + \frac{2}{(e^x - 1)}\right) + D\left(1 + \frac{3}{(e^y - 1)} + \frac{3}{(e^y - 1)^2}\right). \quad (3)$$

The interaction of two phonons can be considered, on the one hand, as the process of scattering of one wave on periodic inhomogeneities created by the second wave, and on the other hand, as the scattering of two particles during their interaction with each other. As a result of the interaction of phonons with frequencies ω_1 and ω_2, a third phonon with frequency $\omega_1 + \omega_2$ arises. Its appearance occurs in accordance with the law of conservation of energy and momentum. Three-phonon processes are related to cubic terms of potential energy expansion. The probability of four-phonon and more processes is significantly less than that of three-phonon processes. Four-phonon processes should play an important role at high temperatures. At high temperatures, multiphonon processes should be taken into account when calculating the thermal resistance [51]. Figure 5, *a, b* show the temperature-dependent Raman spectra of KIn_5S_8. According to expressions (2) and (3), the dependencies $\Delta\omega(T)$ and $\Gamma(T)$ were determined. The analysis showed that the three-phonon process as a whole describes the frequency shift of phonon modes, but for an accurate description of the phonon temperature dependence, four-phonon scattering must be taken into account. However, it is interesting that for a number of modes there is a predominance of four-phonon processes. The values of the fitting parameters are given in Table 3. Similarly to the position of the lines, the dependence of the widths of the spectral lines also corresponds very well to the dominant three-phonon process, and the contribution of four-phonon scattering is less significant. The fitting parameters are given in Table 3. It should be noted that the high phonon density of state (PDOS) of KIn_5S_8 in the range of $\sim 240-300\,cm^{-1}$ (Figure 4) contributes to four-phonon scattering (Table 3) in this frequency range.

Table 3. Comparison of the basic bond lengths (Å) in a crystal of KIn_5S_8 according to single crystal X-ray diffraction (exp.) of a crystal of KIn_5S_8 and according to DFT calculations (calculation)

Bond	KIn_5S_8 (Exp.)	KIn_5S_8 (Calculation.)
K-S1	3.3110(16)	3.33176
K-S2	3.3569(18)	3.22512
In1-S1	2.6346(7)	2.64566
In1-S3	2.6088(4)	2.61361
In3-S4	2.4273(7)	2.44946
In2-S2	2.5903(6)	2.60233

The Raman spectra were measured in the pressure range up to $\sim 10\,GPa$ for the KIn_5S_8 sample (Figure 5, *c, d*). No structural transformations are observed in this range up to $\sim 10\,GPa$. Vibrational modes naturally shift to the high-frequency region. Significant changes in the relative intensity of spectral peaks in the Raman spectra are observed. The most significant changes occur in the area of $\sim 250-350\,cm^{-1}$ (the dotted line in Figure 5, *d* shows these changes), where the collective vibrations of the „mono-ladder“ and of the „bi-ladder“ type are concentrated. At a pressure of $\sim 2\,GPa$, the intensity of the most active peaks in this spectral range is almost equalized. Peaks 299 and $321\,cm^{-1}$ for KIn_5S_8 are completely resolved at $\sim 10\,GPa$. Quite significant changes also occur in the spectral region of $\sim 200\,cm^{-1}$, where intense lines are detected. An „ignition“ of peaks 195 and $201\,cm^{-1}$ is also observed with increasing pressure. A decrease in their relative intensity is also observed.

4.5. Thermodynamic properties

It is necessary to go beyond the harmonic approximation to calculate the thermodynamic properties of a material. For example, it is possible to use the quasi-harmonic approximation (QHA). In this approximation, collective vibrations are described by a set of harmonic oscillators,

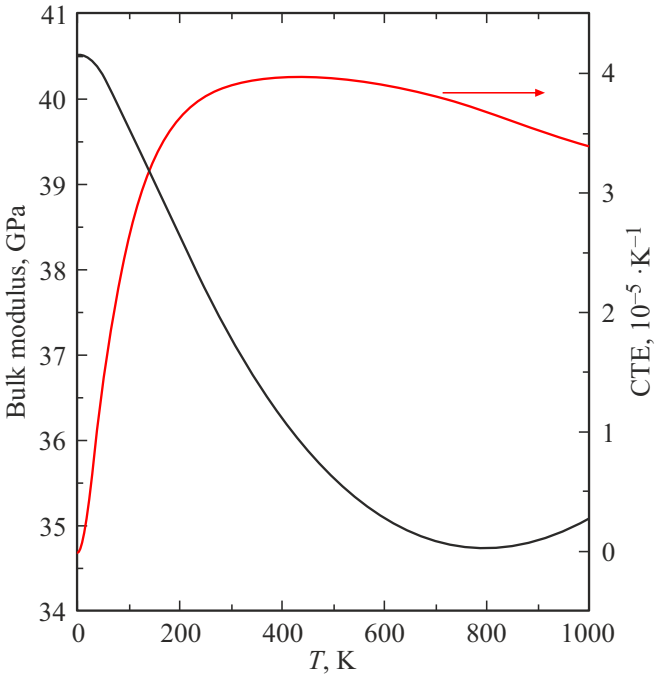

Figure 6. Bulk modulus and coefficient of thermal expansion (CTE) calculated for crystal of KIn_5S_8 in the temperature range of 0–1000 K within the framework of QHA.

and thus the statistical sum can be expressed as an analytical function of crystal volume and temperature. The advantage of this approximation is that all equilibrium thermodynamic properties can be obtained directly. Earlier, this technique was used in Ref. [48] for a series of minerals and showed its validity when reproducing experimental data. The bulk modulus (BM) and the coefficient of thermal expansion (CTE) were calculated in this paper in the temperature range of 0–1000 K within the framework of the QHA approximation (Figure 6).

The CTE value obtained for KIn_5S_8 at 300 K, is equal to $3.90 \cdot 10^{-5}\,K^{-1}$, which is approximately several times higher than the coefficient of thermal expansion of pure yttrium, while the calculated value of the bulk elastic modulus was 37.23 GPa (comparable in magnitude to the elastic properties of amorphous silicon), which indicates the determining influence of phonons on the thermodynamic properties of KIn_5S_8. Moreover, the transport properties are determined by the interaction of phonons, which goes beyond the harmonic approximation.

According to numerous studies in Refs. [53–55], it is known that in temperature-dependent Raman spectra of crystalline materials, the observed phonon frequency shifts are due to a combination of two effects: firstly, the effect of volumetric expansion (implicit), which is associated with changes in interatomic distances and, consequently, with the force constants of bonds; and secondly, there is a purely thermal (explicit) effect associated with the anharmonic interaction of phonons and decay into other phonons at high temperatures (T). For an isotropic crystal, everything described above can be represented by the following expression:

$$\left(\frac{\partial\omega_i}{\partial T}\right)_P = \left(\frac{\partial\omega_i}{V}\right)_T \left(\frac{\partial V}{\partial T}\right)_P + \left(\frac{\partial\omega_i}{T}\right)_V. \quad (4)$$

By rewriting the expression (4) using the compressibility (β) and the coefficient of thermal expansion (α), we can obtain the following (5):

$$\left(\frac{\partial\omega_i}{\partial T}\right)_P = -\left(\frac{\beta(T)}{\alpha(T)}\right)\left(\frac{\partial\omega_i}{\partial P}\right)_T + \left(\frac{\partial\omega_i}{\partial T}\right)_V. \quad (5)$$

The Grüneisen mode parameter is a measure of the anharmonicity of phonon modes and is directly related to the third-order force constants [56,57]. The dependence of the phonon frequency on pressure is expressed by the Grüneisen isothermal parameter $\gamma_{i,T}$, defined as:

$$\gamma_{i,T} = -\frac{1}{\beta\omega_i}\left(\frac{\partial\omega_i}{\partial P}\right)_T, \quad (6)$$

where β is compressibility. Similarly, the Grüneisen isobaric parameter $\gamma_{i,P}$ is expressed as:

$$\gamma_{i,P} = -\frac{1}{\alpha\omega_i}\left(\frac{\partial\omega_i}{\partial T}\right)_P. \quad (7)$$

In this regard, the expression (5) can be rewritten as:

$$\frac{1}{\omega_i}\left(\frac{\partial\omega_i}{\partial T}\right)_i = \alpha\gamma_{i,T} + \frac{1}{\omega_i}\left(\frac{\partial\omega_i}{\partial T}\right)_V. \quad (8)$$

In a global analysis of the bond structure in a crystal lattice, the semiempirical coefficient η can be defined as [56]:

$$\eta = \frac{\gamma_{iT}}{\gamma_{iP}}, \quad (9)$$

which is a quasi-harmonic fraction of the material. At $\eta < 0.5$, it is assumed that there is a significant influence of anharmonicity on the frequency of phonons at temperatures other than absolute zero, and at $\eta \approx 1$ ($\gamma_{i,T} \approx \gamma_{i,P}$), it is assumed that the anharmonic contribution will tend to zero [56–58], and thermal expansion is described in the approximation without taking into account the interaction of phonons, which is the harmonic approximation. The availability of experimental data on the dependences of thermal and baric spectral parameters KIn_5S_8 makes it possible to analyze the dynamics of the crystal lattice. In Table 4, for many phonon modes KIn_5S_8, the explicit contribution of anharmonicity prevails over the net volume or the implicit contribution of anharmonicity for Raman-active modes, for which the values of the quasi-harmonic fraction are on average $\eta \sim 0.3$. It is assumed that the presence of modes with pronounced anharmonicity may also indicate a decrease in thermal conductivity due to phonon-phonon scattering.

Table 4. Parameters for fitting the temperature dependences of the positions (ω) and widths (Γ_{exp}) of lines in the Raman spectrum of the crystal of KIn_5S_8 in the temperature range of 83−773 K; IR — irreducible representation; ω_0, A, B, Γ_0, C, D fitting parameters according to [52]

ω, cm^{-1}	IR	ω_0, cm^{-1}	A, cm^{-1}	B, cm^{-1}	Γ_{exp}, cm^{-1}	Γ_0, cm^{-1}	$C \cdot 10^{-2}$, cm^{-1}	$D \cdot 10^{-5}$, cm^{-1}
126	*A*	127.4	0.17	−0.017	4.2	1.3	0	0.45
140	*A*	141.4	−0.11	−0.008	4.4	1.0	0.45	0
195	*A*	201.2	−0.42	−0.07	9.2	4.4	2.0	1.0
201	*A*	209.6	−1.8	0	0.3	0.4	0.44	0
240	*A*	246.4	−1.15	−0.035	12.4	1.5	2.0	0
255	*A*	264.0	−1.05	−0.15	10.2	2.1	1.7	0.50
286	*A*	298.8	2.4	−0.4	–	–	–	–
299	*A*	305.4	−0.35	−0.4	12.6	2.7	3.0	0
321	*A*	322.5	−0.03	−0.14	14.7	1.9	3.3	−0.90
363	*A*	369.0	−0.3	−0.38	8.4	4.0	0.30	5.0

Table 5. Experimental values of vibrational mode frequencies (ω) for a crystal of KIn_5S_8 and their irreducible representations; γ_{iT}, γ_{iP}, γ_{iV} — isothermal, isobaric, and volumetric Grüneisen parameters (at $T = 300$ K); contributions of thermal expansion — $-\frac{\beta}{\alpha}\left(\frac{\partial\omega_i(T)}{\partial P}\right)_T$ and phonon-phonon interaction $\left(\frac{\partial\omega_i(T)}{\partial T}\right)_V$ to general anharmonicity $\left(\frac{\partial\omega_i(T)}{\partial T}\right)_P$; $\eta = \gamma_{iT}/\gamma_{iP}$

ω, cm^{-1}	IR	γ_{iT}	γ_{iP}	γ_{iV}	$\left(\frac{\partial\omega_i(T)}{\partial T}\right)_P$	Implicit. $-\frac{\beta}{\alpha}\left(\frac{\partial\omega_i(T)}{\partial P}\right)_T$	Explicit $\left(\frac{\partial\omega_i(T)}{\partial T}\right)_V$	η
140	*A*	0.71	0.96	0.25	−0.005	−0.004	−0.001	0.7
195	*A*	0.96	2.80	1.94	−0.021	−0.007	−0.015	0.3
201	*A*	0.77	2.87	2.10	−0.023	−0.006	−0.016	0.3
240	*A*	1.07	1.28	0.20	−0.012	−0.010	−0.002	0.8
255	*A*	0.45	3.06	2.61	−0.031	−0.004	−0.026	0.1
299	*A*	0.67	1.03	0.36	−0.012	−0.008	−0.004	0.7
321	*A*	0.86	0.77	−0.09	−0.010	−0.011	0.001	1.1
363	*A*	0.65	1.80	1.15	−0.026	−0.009	−0.016	0.4

The presence of appropriate thermodynamic characteristics allowed us to estimate the thermal properties of KIn_5S_8. The phenomenological expression for the thermal conductivity of the lattice due to phonon-phonon scattering is defined as [59,60]:

$$\kappa_L = A\frac{\langle M\rangle\theta_D^3\delta}{\gamma_a^2 n^{2/3}T}, \tag{10}$$

where κ_L is the thermal conductivity of the crystal lattice, $\langle M\rangle$ is the average atomic mass, n is the number of atoms in a unit cell, δ is the volume per atom, T is the temperature, γ_a is the average Grüneisen parameter for acoustic branches, θ_D is the Debye temperature, A is the value, associated with the Grüneisen parameter γ_a is equal to:

$$A = \frac{2.43 \cdot 10^6}{1 - \frac{0.514}{\gamma_a} + \frac{0.228}{\gamma_a^2}}. \tag{11}$$

The average value of the Grüneisen parameter for acoustic branches was 0.90 for KIn_5S_8. The Debye temperature θ_D is determined by approximating the temperature dependence of the heat capacity Cv. Thus, the Debye temperature θ_D for $KIn_5S_8$is 82.5 K, the Grüneisen parameter for acoustic branches γ_a is found to be 0.90. Using the expression (10) for the crystal of KIn_5S_8, the value of the thermal conductivity of the lattice at 300 K was calculated as 0.41 W/(mK).

Despite the fact that the obtained value of thermal conductivity using the empirical expression (10) is of an estimated nature, it already allows us to classify KIn_5S_8 as a class of materials with low ionic conductivity and encourage researchers to study the thermodynamic properties of the material in more depth. In the future, the authors plan to carry out a more detailed calculation of thermodynamic properties in a rather resource-intensive approximation of time relaxation, which will be discussed in a separate publication.

5. Conclusion

KIn_5S_8 crystals were synthesized by the solution-melt method in this study. Taking into account the contradictions in the data on the crystal structure of KIn_5S_8, using a proven approach involving distortion of the structure along the vectors of atomic displacements of an unstable mode with an imaginary frequency for KIn_5S_8 the DFT calculations indicate several stable structures, namely *P-1* (N 2), $P2_1$ (N 4), $P2_1/c$(N 14). The dynamic properties of KIn_5S_8 are analyzed. Data on the interpretation of experimental Raman spectra on this basis have been obtained. Combining thermal and baric Raman spectroscopy data from KIn_5S_8 crystal and using an approach related to the representation of general anharmonicity (phonon frequency shift with increasing temperature) by volume expansion (implicit contribution) and phonon-phonon interaction (explicit contribution), it is shown that for most phonon modes, the explicit contribution of anharmonicity prevails over the implicit contribution for Raman-active modes (values of the quasi-harmonic fraction $\eta \sim 0.3$). Estimates of thermal conductivity by phenomenological expression were 0.41 W/(mK) at 300 K, which is lower than for compounds of similar classes (for example, for $AgIn_5S_8$ $\kappa_L = 0.97$ W/(mK)). Such low values of thermal conductivity already at 300 K for simple crystal systems opens up wide opportunities for the development of efficient thermoelectric systems.

Acknowledgments

The study was performed using computing resources of the supercomputer in Ioffee Physical-Technical Institute. Experimental data were obtained at the CUC „Geoanalytik“ (Institute of Geology and Geochemistry, Ural Branch of the Russian Academy of Sciences).

Funding

The study was supported by the Russian Science Foundation grant No. 24-73-00009 (https://rscf.ru/project/24-73-00009/).

Conflict of interest

The authors declare that they have no conflict of interest.

References

[1] J.P. Heremans. Nature Phys. **11**, 990 (2015).
[2] R. Mittal, M. Gupta, S. Chaplot. Prog. Mater. Sci. **92**, 360 (2018).
[3] C.W. Li, J. Hong, A.F. May, D. Bansal, S. Chi, T. Hong, G. Ehlers, O. Delaire. Nature Phys. **11**, 1063 (2015).
[4] B. Wei, Q. Sun, C. Li, J. Hong. Sci. China Phys. Mech. Astron. **64**, 117001 (2021).
[5] M. Christensen, A.B. Abrahamsen, N.B. Christensen, F. Juranyi, N.H. Andersen, K. Lefmann, J. Andreasson, C.R. Bahl, B.B. Iversen. Nature Mater. **7**, 811 (2008).
[6] M. Balkanski, R. Wallis, E. Haro. Phys. Rev. B **28**, 1928 (1983).
[7] H.-J. Pang, L.-C. Chen, Z.-Y. Cao, H. Yu, C.-G. Fu, T.-J. Zhu, A.F. Goncharov, X.-J. Chen. J. Appl. Phys. **124**, 135102 (2018).
[8] B. Karki, R.D. Wentzcovitch, S. De Gironcoli, S. Baroni. Science **286**, 1705 (1999).
[9] A. Erba, M. Shahrokhi, R. Moradian, R. Dovesi. J. Chem. Phys. **142**, 204501 (2015).
[10] A.M. Medina-Gonzalez, P. Yox, Y. Chen, M.A. Adamson, B.A. Rosales, M. Svay, E.A. Smith, R.D. Schaller, K. Wu, A.J. Rossini et al. Chem. Mater. **34**, 7357 (2022).
[11] H. Yu, L.-C. Chen, H.-J. Pang, P.-F. Qiu, Q. Peng, X.-J. Chen. Phys. Rev. B **105**, 245204 (2022).
[12] M.D. Ward, E.A. Pozzi, R.P. Van Duyne, J.A. Ibers. J. Solid State Chem. **212**, 191 (2014).
[13] V. Winkler, M. Schlosser, A. Pfitzner, Z. Anorg. Allg. Chem. **641**, 549 (2015).
[14] H.-Y. Zeng, M.-J. Zhang, B.-W. Liu, N. Ye, Z.-Y. Zhao, F.-K. Zheng, G.-C. Guo, J.-S. Huang. J. Alloys Compd. **624**, 279 (2015).
[15] K. Feng, D. Mei, L. Bai, Z. Lin, J. Yao, Y. Wu. Solid State Sci. **14**, 1152 (2012).
[16] L. Isaenko, I. Vasilyeva, A. Merkulov, A. Yelisseyev, S. Lobanov. J. Cryst. Growth **275**, 217 (2005).
[17] L. Isaenko, A. Yelisseyev, S. Lobanov, V. Petrov, F. Rotermund, G. Slekys, J.-J. Zondy. J. Appl. Phys. **91**, 9475 (2002).
[18] L. Isaenko, A. Yelisseyev, S. Lobanov, A. Titov, V. Petrov, J.-J. Zondy, P. Krinitsin, A. Merkulov, V. Vedenyapin, J. Smirnova. Cryst. Res. Technol. **38**, 379 (2003).
[19] V. Atuchin, L. Isaenko, V. Kesler, S. Lobanov. J. Alloys Compd. **497**, 244 (2010).
[20] X. Lin, G. Zhang, N. Ye. Cryst. Growth Des. **9**, 1186 (2009).
[21] J. Yao, D. Mei, L. Bai, Z. Lin, W. Yin, P. Fu, Y. Wu. Inorg. Chem. **49**, 9212 (2010).
[22] J. Yao, W. Yin, K. Feng, X. Li, D. Mei, Q. Lu, Y. Ni, Z. Zhang, Z. Hu, Y. Wu. J. Cryst. Growth **346**, 1 (2012).
[23] D. Mei, W. Yin, L. Bai, Z. Lin, J. Yao, P. Fu, Y. Wu. Dalton Trans. **40**, 3610 (2011).
[24] M.-Y. Kim, W.-T. Kim, M.-S. Jin, S.-A. Park, S.-H. Choe, C.-I. Lee, S.-C. Hyun, C.-D. Kim. J. Phys. Chem. Solids **64**, 625 (2003).
[25] B. Tagiev, S. Abushov, O. Tagiev. J. Appl. Spectrosc. **77**, 115 (2010).
[26] Y. Begum, S. Khan, A.H. Reshak, A. Laref, Z. Amir, G. Murtaza, J. Bila, M.R. Johan, T.H. Al-Noor. Int. J. Energy Res. **45**, 4014 (2021).
[27] D. Friedrich. Synthese, Strukturchemie, Eigenschaften und Hochtemperaturverhalten neuer Chalkogenogallate der schweren Alkalimetalle, dissertation (2018).

[28] H. Deiseroth. Z. Kristallogr. **177**, 307 (1986).
[29] H. Deiseroth, C. Reiner. Z. Anorg. Allg. Chem. **624**, 1839 (1998).
[30] A. Jain, S.P. Ong, G. Hautier, W. Chen, W.D. Richards, S. Dacek, S. Cholia, D. Gunter, D. Skinner, G. Ceder et al. APL Mater. **1**, 011002 (2013).
[31] D.A. Chareev. Kristallografiya **61**, 475 (2016) (in Russian).
[32] D.A. Chareev, O.S. Volkova, N.V. Geringer, A.V. Koshelev, A.N. Nekrasov, V.O. Osadchy, O.N. Filimonova. Kristallografiya **61**, 652 (2016) (in Russian).
[33] V. Petříyek, M. Dušek, L. Palatinus. Z. Kristallogr. **229**, 345 (2014).
[34] X. Chen, B. Zhao, T. Tang, X. Yin, R. Li, D. Han. J. Chem. Thermodyn. **163**, 106592 (2021).
[35] G. Kresse, J. Hafner. Phys. Rev. B **49**, 14251 (1994).
[36] G. Kresse, J. Furthmüller. Comput. Mater. Sci. **6**, 15 (1996).
[37] J.P. Perdew, K. Burke, M. Ernzerhof. Phys. Rev. Lett. **77**, 3865 (1996).
[38] P.E. Blöchl. Phys. Rev. B **50**, 17953 (1994).
[39] G. Kresse, D. Joubert. Phys. Rev. B **59**, 1758 (1999).
[40] H.J. Monkhorst, J.D. Pack. Phys. Rev. B **13**, 5188 (1976).
[41] M. Ferrero, M. Rérat, B. Kirtman, R. Dovesi. J. Chem. Phys. **129**, 244110 (2008).
[42] R. Dovesi, A. Erba, R. Orlando, C.M. Zicovich-Wilson, B. Civalleri, L. Maschio, M. Rérat, S. Casassa, J. Baima, S. Salustro, B. Kirtman. WIREs Comput. Mol. Sci. **8**, e1360 (2018).
[43] M.F. Peintinger, D.V. Oliveira, T. Bredow. J. Comput. Chem. **34**, 451 (2013).
[44] J.P. Perdew, A. Ruzsinszky, G.I. Csonka, O.A. Vydrov, G.E. Scuseria, L.A. Constantin, X. Zhou, K. Burke. Phys. Rev. Lett. **100**, 136406 (2008).
[45] A. Togo, L. Chaput, T. Tadano, I. Tanaka. J. Phys.: Condens. Matter **35**, 353001 (2023).
[46] A. Togo, I. Tanaka. Scripta Mater. **108**, 1 (2015).
[47] E.M. Roginsky, Yu.F. Markov, A.I. Lebedev. ZhETF **155**, *5*, 855 (2019) (in Russian) .
[48] E.M. Roginsky, A.V. Savin, E.A. Pankrushina. FTT **67**, *5*, 823 (2025) (in Russian).
[49] G.H. Wolf, R. Jeanloz. J. Geophys. Res. **89**, 7821 (1984).
[50] N.P. Salke, M. Gupta, R. Rao, R. Mittal, J. Deng, X. Xing. J. Appl. Phys. **117**, 155901 (2015).
[51] Y. Joshi, M. Tiwari, G. Verma. Phys. Rev. B **1**, 642 (1970).
[52] P. Klemens. Phys. Rev. **148**, 845 (1966).
[53] F. Cerdeira, F. Melo, V. Lemos. Phys. Rev. B **27**, 7716 (1983).
[54] E. Sarantopoulou, C. Raptis, S. Ves, D. Christofilos, G. Kourouklis. J. Phys.: Condens. Matter **14**, 8925 (2002).
[55] L.-C. Chen, Z.-Y. Cao, H. Yu, B.-B. Jiang, L. Su, X. Shi, L.-D. Chen, X.-J. Chen. Appl. Phys. Lett. **113**, 251902 (2018).
[56] I.R. Amaral, D.M. Vasconcelos, A.G. Souza Filho, V.V. Oliveira, R.S. Alencar, A.S. de Menezes, R.L. Lobato, L.A. Montoro. J. Raman Spectrosc. **54**, 781 (2023).
[57] G. Lucazeau. J. Raman Spectrosc. **34**, 478 (2003).
[58] R. Zallen, E. Conwell. Solid State Commun. **31**, 557 (1979).
[59] G.A. Slack. J. Phys. Chem. Solids **34**, 321 (1973).
[60] D.T. Morelli, G.A. Slack. High Lattice Thermal Conductivity Solids. In: Shindé, S.L., Goela, J.S. (eds) High Thermal Conductivity Materials. Springer, New York (2006). P. 37–68

Translated by A.Akhtyamov